Engineering and Technology Journal
Journal homepage: https://etj.uotechnology.edu.iq

Investigating the effect of cooling systems on the efficiency of photovoltaic solar panels

Bilal Y. Dawood Al-Asbea

Islamic Azad University, Shiraz branch, Renewable Energy Engineering, Iran.
*Corresponding author Email: bilalyahea0@gmail.com

HIGHLIGHTS

- The study examined the effect of cooling systems on the efficiency of photovoltaic solar panels
- Thermal efficiency improved and fluid strain loss reduced by adding flow-guiding obstacles in the chamber
- The new configuration reduced pressure drop and minimized fluid vortices inside the cooling chamber
- Optimal performance was achieved using well-placed flow-guiding obstacles

Keywords:
Photovoltaic solar panels
Cooling systems
Nanofluids
ANSYS fluent simulation
Multi-objective optimization

ABSTRACT

This research investigates the influence of cooling systems on the performance of photovoltaic (PV) solar panels, specifically using pulsing tubes filled with alumina and titanium dioxide nanofluids under conditions characteristic of solar power plants. Cooling photovoltaic (PV) solar panels is essential for improving their efficiency in solar generating facilities. This work examines the use of pulsing tubes containing Al_2O_3 and TiO_2 nanofluids, together with flow-guiding barriers, to enhance cooling efficiency. Through ANSYS Fluent simulations, we determined that two barriers decrease panel temperature by around 20% (from 60 °C to 48 °C), enhance heat transmission by around 30%, and augment efficiency by about 7% relative to the absence of obstacles. Al_2O_3 nanofluid surpasses TiO_2, achieving a temperature reduction of 22% compared to 18%. Pressure drop decreases by ~15% with two obstacles, improving fluid dynamics. These results indicate that efficient cooling solutions may substantially improve photovoltaic panel performance by up to 10%. The project aims to enhance thermal efficiency and minimize fluid strain loss by directing obstacles inside the cooling chamber. Simulations were conducted using ANSYS Fluent, and the results have been validated using empirical data. The study showed that incorporating steering obstacles produced optimal results, significantly reducing panel surface temperature, increasing heat transfer, and improving the cooling fluid's temperature homogeneity. This layout decreased pressure loss and minimized fluid vortices inside the chamber, resulting in enhanced heat transfer and performance, in contrast to configurations without impediments or featuring a single impediment. The results demonstrated optimal machine performance by implementing guiding constraints, whereas low efficiency was seen without such bounds. Furthermore, efficiency decreased around noon when solar radiation reached its zenith due to increased panel temperatures, but subsequently improved when the panels cooled in the following hours. The findings suggest adjusting flow-guiding barriers to improve the efficiency of solar panels under actual operating circumstances.

1. Introduction

The use of fossil fuel-powered power generation systems is one factor contributing to the production of greenhouse gases. Therefore, considering the geographic position of our country and the potential of solar energy, its use for a range of applications may have a special place among renewable energy sources. One of these uses is power generation, which is accomplished via photovoltaic solar collectors. Conventional solar collectors fall into one of three categories based on their geometry: evacuated tube (ETC), flat plate (FPC), or composite pair (CPC) [1].

In the study by Hosseini et al. [2], putting a thin layer of water in front of a monocrystalline panel increased the solar system's total efficiency by 1%. This experiment was conducted with a 0.44 m^2 panel area, a one lpm water flow rate, a 0.25 horsepower pump, and a 20 °C panel temperature. Two aluminium tubes were used by Du et al. [3], to cool the back of a monocrystalline panel that measured 0.152 m^2. At a water wafting rate of 0.035 kg/s, they could boost the panel temperature to 60 °C while decreasing efficiency by 0.8%. Additionally, Bahaidarah et al. [4], noted a temperature drop of 10 °C and a 2.8% growth in performance whilst cooling a 1.24 m^2 monocrystalline module with a pump electricity consumption of 0.5 hp and a waft rate of

http://doi.org/10.30684/etj.2025.159652.1950
Received 29 April 2025; Received in revised form 02 June 2025; Accepted 05 June 2025; Available online 25 July 2025
2412-0758/University of Technology-Iraq, Baghdad, Iraq

0.06 kg/s. Xu et al. [5], verified that cooling with nanofluid has more capability than cooling with water and that electrical performance rises by growing a numerical model for each water and nanofluid. A Peltier-impact-based thermoelectric cooling tool for targeted sun cells was also simulated by Najafi et al. [6], who concluded it's suitable for optimizing the photovoltaic module's overall performance. Hachicha et al. [7], compared the back and front cooling of the module and determined that the front cooling successfully reduces the module's temperature. Alboteanu et al. [8], computationally simulated the warmth delivery of the behind-the-module cooling approach using Quick Field software. They showed a considerable growth in the output power of the solar module. This looks at the importance of several cooling techniques in increasing the efficiency of solar structures, including the Peltier effect, water, and nanofluids.

A dual-axis tracking system and a high-concentration photovoltaic system prototype with a concentration ratio of 11 were introduced by Rosell et al. [9], in 2005. This device demonstrated more than 60% thermal efficiency by combining a Fresnel linear concentrator with a channel photovoltaic/thermal collector. The thermal conductivity between the absorber plate and the PV cells is a crucial factor in enhancing performance, as this study verified using an analytical model to forecast the system's thermal behaviour. In 2006, Cheknane et al. [10], used a gravity-dependent copper heat pipe to study the function of passive cooling. Using acetone as the working fluid enhanced the concentrator cells' performance by up to 500× and demonstrated how cost-effective it is to put such high-efficiency systems into place. Grey et al. [11], also provided a theoretical model of the passive cooling system in Ammonix HCPV systems in 2007 using experimental data and Gambit software. The findings show that eliminating waste heat from the cells enhances their functionality in adverse weather and at high concentrations. Ouhib et al. [12], focused their research on the POPT polymer in 2008 to investigate the effects of phenyl groups on thermal and photovoltaic properties. The outcomes showed that the aggregate of those polymers enhances thermal stability, reduces the tendency for crystallisation, and improves light absorption properties within the near-infrared region. The effectiveness of drying structures with hybrid photovoltaic-thermal collectors in warm, humid regions was examined via Beccali et al., [13]. Solar cooling systems with PV/t collectors can produce warmth and power simultaneously, resulting in massive energy monetary savings and high monetary overall performance, consistent with a comprehensive energy and financial evaluation. Dong et al. [14], proposed and investigated a unique multi-channel cooling manifold for centered photovoltaic (CPV) structures. The cooling medium, the inlet float fee, and the channel diameters significantly affect thermal performance, which aligns with the findings. This technology furnished higher cooling performance with temperature homogeneity and lower thermal resistance than those reported in the literature. The coupling among solar radiation, PV cell temperature, and tool performance was investigated in the 2019 study by Rocha et al., [15]. In addition to the thermal strength era, the most important factor (MPP) voltage has been made more solid and rate-effective by using a suitable cooling device to stabilise the PV module temperature and streamline the MPPT algorithms [16, 17]. Abou-Ziyan et al. [18], examined a developed simple and reasonably priced microchannel cooling solution for high-attention multi-junction PV cells. This gadget validated brilliant improvements over today's systems regarding overall thermal performance and power technology. The -stage microchannel machine confirmed the most temperature consistency, despite the constant-width microchannel gadget having a higher strength output and reduced thermal resistance. Torbatinezhad et al. [19], study also looked at a computer model of a concentrated photovoltaic system's pin-finned reinforced heat sink. To attain maximal exergy, the fin angle was increased, the heat sink temperature decreased, and thermal and electrical efficiency increased by 80% and 29%, respectively. In the 2022 project, Sornek et al. [20], evaluated and tested a water cooling system for photovoltaic panels. In practice, this method reduced the panel temperature by 24 K and increased the power production by 10%.

By optimising the relevant parameters, ambitions are looked at to minimise fluid strain loss and maximise thermal performance. It examines the outcomes of using pulsating tubes sporting alumina and titanium dioxide nanofluids in photovoltaic panel cooling with boundary conditions from solar power flora. A parametric analysis was completed to analyze the consequences of geometrical and bodily parameters on pulsating glide after the panel with special shapes was designed and simulated. The numerical effects had been established through the use of experimental information.

Most previous investigations have focused on conventional cooling techniques or applying a single nanofluid in simplified cooling channel geometries. The combined effect of advanced heat transfer fluids—specifically dual nanofluids—and innovative flow management techniques, such as integrating pulsating tubes and flow-guiding obstacles, remains insufficiently explored. In particular, the synergistic impact of simultaneously optimizing fluid composition and internal chamber structure on the thermal and electrical performance of PV modules under representative outdoor conditions is not addressed in existing literature.

The present study aims to bridge this gap by systematically investigating the impact of pulsating tube cooling configurations filled with alumina (Al_2O_3) and titanium dioxide (TiO_2) nanofluids, individually and in combination, alongside strategically placed internal guide obstacles. The research deploys high-fidelity ANSYS Fluent simulations validated against experimental data, uniquely analyzing how dual nanofluid mixtures and flow-guiding structures affect heat transfer, temperature uniformity, pressure drop, and PV efficiency.

- **Pulsating Tubes:** For the first time in this context, the application of pulsating tubes aims to enhance fluid mixing and heat exchange efficiency within the cooling chamber.
- **Dual Nanofluids:** The study explicitly compares and combines two distinct nanofluids (Al_2O_3 and TiO_2), studying their individual and coupled thermal effects.
- **Guide Obstacles:** The geometric optimization and systematic placement of guide obstacles within the cooling flow path is introduced as a novel mechanism to maximize surface contact, disrupt thermal boundary layers, and homogenize temperature distribution.

Through this integrated approach, the current research delivers new insights into the multi-parameter optimization of PV panel cooling—a significant advancement towards efficient, deployable, and economically viable solar energy solutions.

This study accomplished multi-goal optimisation, which included decreasing the pressure drop in the cooling waft and improving the efficiency of electricity generation. It used a genetic set of rules and the multi-goal MDO technique. This method permits the fulfillment of the excellent design objectives by refining preliminary facts and evaluating the most desirable responses.

2. Governing equations

2.1 Nominal operating cell temperature

The Nominal Operating Cell Temperature (NOCT) is the conditions for a photovoltaic (PV) cell to operate at: 800 W/m² solar irradiation, atmospheric temperature of 20 °C, and wind speed of 1 m/s. This parameter assists in determining the PV cell effectiveness curve in different thermal conditions. This was the phrase "The Nominal Operating Cell Temperature," which was then corrected for clarity. A key indicator for predicting how much a PV mobile's temperature will differ because of solar radiation and ambient temperature is NOCT, which is impacted by module design, creation materials, and packing density. The manufacturing generation and module producer affect the NOCT fee, which ranges from 45 °C to 48 °C.

Each PV module has a personal temperature coefficient that determines how temperature variations affect output energy, voltage, and cutting-edge. The temperature coefficient of voltage (HV), usually -3.7×10⁻³ mV/°C, is the quantity the open-circuit voltage decreases with every degree of temperature change. The temperature coefficient of modern (HI) describes the temperature-brought about boom in brief-circuit cutting-edge (6.4×10⁻⁴ mA/°C), and the temperature coefficient of energy (HP) is calculated the usage of the maximum electricity factor voltage and HV. These equations analyse the PV module's thermal performance under real-world working situations.

It calculates how much a PV module's open circuit voltage fluctuates in response to temperature changes as in Equation (1) [20]:

$$H_V = -3.7 \times 10^{-3}\ mV/1℃ \tag{1}$$

A PV module's short-circuit current alternates due to temperature changes and is measured via the modern temperature coefficient H_I, as in Equation (2) [21]:

$$H_I = 6.4 \times 10^{-4}\ mA/1℃ \tag{2}$$

The power shift delivered via a change in PV temperature is measured with the aid of the temperature coefficient of energy, or H_P. The following method [22] can be used to estimate it using the temperature coefficient of H_V voltage as in Equation (3):

$$H_P = \frac{H_V}{V_{mp}} \tag{3}$$

The temperature coefficient of open circuit voltage, or H_V, is expressed as V/°C. Under typical test settings, V_{mp} equals the voltage at the maximum power point. Since the cell's temperature influences the primary coefficient, the temperature coefficient of voltage is often included with the module data sheet from the manufacturer.

2.2 Influence of temperature on solar cells

Temperature impacts solar cells, where the open circuit voltage decreases by 3.7 × 10⁻³ mV/°C as the temperature increases [23]. All semiconductor devices, including solar cells, are impacted by temperature. The band gap of a semiconductor shrinks as the temperature rises, affecting most of the material's properties. An increase in the electron energy of a semiconductor can be thought of as a decrease in the band gap as the temperature rises. Consequently, less energy is needed to break the bond. The semiconductor band gap bonding principle shows that decreasing binding energy reduces the band gap. As a result, the band gap shrinks with increasing temperature. Greater diode current since I_0 is subtracted from the radiation-generated current in equations 3-4, it denotes higher cell operation losses. I_0 is one of the variables that affects the open circuit voltage, and the equation that follows [24] shows how the open circuit voltage decreases with increasing temperature as shown in Equations (4 and 5):

$$V_{OC} = \frac{kT}{q} \ln \frac{I_{SC}}{I_O} \tag{4}$$

$$I_O = qA \frac{Dn_i^2}{LN_D} \tag{5}$$

One crucial factor in silicon that greatly affects temperature-dependent semiconductor conduct is the intrinsic carrier concentration, or ni. It is stricken by the energy of the carriers, which rises with temperature, and the band hole energy, in which smaller band gaps bring about large intrinsic carrier concentrations. The intrinsic provider concentration equation governs the relationship between nini and temperature, wherein nini reveals a strong exponential dependence on the band hole power. As the temperature rises, the companies' power will increase, leading to a better intrinsic carrier concentration due to more desirable thermal excitation. This exponential growth of nini with temperature overshadows other parameters, including doping density (ND) and minority carrier diffusion (D), which exhibit comparatively minimum temperature dependence. Consequently, the

intrinsic service awareness becomes dominant in know-how temperature outcomes on silicon cloth residences and the overall performance of electronic devices as shown in Equation (6):

$$n_i^2 = 4\left(\frac{2\pi kT}{h^2}\right)^3 (m_c m_h)^{\frac{3}{2}} \exp\left(-\frac{E_{G0}}{k_T}\right) = BT^3 \exp\left(-\frac{E_{G0}}{kT}\right) \quad (6)$$

The intrinsic carrier concentration nini is intrinsically tied to fundamental constants and cloth houses, displaying a dependence on temperature and diverse bodily parameters. Key constants, including Planck's constant h=6.626×10^{-34}J and Boltzmann's constant okay=1.3806×10^{-23} J/K, along with the effective masses of electrons (mcmc) and holes (mhmh), collectively form the thermal excitation method in semiconductors. The band gap (EG_0), extrapolated to absolute 0 temperature, is an important element influencing carrier technology, with smaller values selling higher service concentrations. Additionally, the parameter BB, an almost temperature-unbiased consistent, contributes to modeling carrier awareness behavior. Together, these parameters define the mechanisms of thermal equilibrium and enable a deeper understanding of temperature effects on semiconductor materials and device performance.

The effect of I_0 on the open circuit voltage can be calculated in Equation (7).

$$V_{OC} = \frac{kT}{q}\ln\left(\frac{I_{SC}}{I_O}\right) = \frac{kT}{q}[\ln I_{SC} - \ln I_O\,] = \frac{kT}{q}\ln I_{SC} - \frac{kT}{q}\ln\left[B'T^{\gamma}\exp\left(-\frac{qV_{G0}}{kT}\right)\right] \rightarrow$$

$$V_{OC} = \frac{kT}{q}\left(\ln I_{SC} - \ln B' - \gamma \ln T + \frac{qV_{G0}}{kT}\right) \quad (7)$$

where k is the Boltzmann constant (1.38 × 10^{-23} J/K), q is the electron charge (1.6 × 10^{-19} C), T is the temperature in Kelvin, I_sc is the short-circuit current, I_o is the saturation current, and I_L is the light-generated current. For simplicity, V/ °C can be approximated as (kT/q) * ln(I_sc/I_o) under low I_L conditions. The short circuit current I_sc for Si increases slightly by around 0.0006 A/ °C, as the open circuit voltage falls with increasing temperature. An estimate of how temperature affects maximum power is ~0.004 to ~0.005 V/°C for a PV module with 50 cells, roughly 2 × 50 = 110 mV/°C. These numbers are for a single silicon solar cell [24].

2.3 Heat generation and heat loss in PV modules (solar cells)

A typical commercial solar module operating at maximum power converts 10 to 15 percent of the sunshine into electricity, with the remaining portion converted to heat. Consequently, when a photovoltaic module is exposed to sunlight, it generates heat and energy. The following factors influence heat generation (module heating):

- The solar cells' absorption of low-energy, or infrared, light.
- The cells' electrical performance, or the current passing through the series and shunt resistors.
- The top surface's reflection.
- The voids are module regions where sunlight is absorbed but not covered by a solar cell.
- The components of the solar cell packs.

Conduction losses are due to contact between the PV module and other materials, including the surrounding air. The ability to transfer heat depends on the thermal resistance and configuration of the materials used to cover the solar cells and the materials in contact with the module as shown in Equation (8).

$$q = \frac{K_T}{s} \times A(T_{SC} - T_{am}) \quad (8)$$

Air flow across the PV module's surface causes convection heat loss. The following Equation (9) provides it:

$$q = h_c A(T_{sc} - T_{am}) \quad (9)$$

Losses from radiation since the PV module, like any other item, emits radiation (heat) based on its temperature, the final method of heat loss is radiative. The following formula Equation (10) can be used to represent the heat lost via radiation:

$$q = \varepsilon\sigma A(T_{SC}^4 - T_{am}^4) \quad (10)$$

3. Panel electrical efficiency

In numerical analysis, the electrical energy efficiency of the PVT system can be estimated by an empirical relationship presented by Evans [24] as follows in Equation (11):

$$\eta_{el} = \frac{\dot{E}_{el}}{\dot{E}_{sun}} = \eta_r[1 - 0.0045(T_{cell} - 298.15)] \quad (11)$$

In this regard, η_r represents the efficiency of the photovoltaic module under standard test conditions, which is considered equal to 15 °C in this study [24], and T_{cell} is the cell temperature.

3.1 Nanofluid properties and governing equations

Nanofluids, consisting of water with 1% volume fraction of alumina (Al_2O_3) or titanium dioxide (TiO_2) nanoparticles, enhance cooling due to their high thermal conductivity. Table 1 lists their thermophysical properties:

Table 1: Thermophysical properties of water and nanoparticles (Al_2O_3 and TiO_2) for nanofluid applications

Material	Density (kg/m³)	Thermal conductivity (W/m·K)	Specific heat (J/kg·K)
Water	998	0.60	4180
Al_2O_3 (Aluminum Oxide)	1028	0.65	4120
TiO_2 (Titanium Dioxide)	1015	0.62	4150

The nanofluid properties are calculated as follows:

1) Density: $\rho\_nf = (1 - \varphi)\rho\_f + \varphi\rho\_p$
2) Thermal Conductivity: $k\_nf = k\_f\,(1 + 2.5\varphi)$

Simulations showed that Al_2O_3 nanofluid reduces panel temperature by 22% (to 45 °C) and TiO_2 by 18% (to 48 °C) compared to water (52 °C). illustrates the temperature distribution for each fluid.

4. Panel geometry and boundary conditions

For the analysis of this research, a photovoltaic panel with dimensions of 1.5 × 1 m² is designed. This panel has several layers: glass, EVA, photovoltaic cells, EVA, Tedlar, and finally, a copper interface plate placed between the Tedlar and the cooling plate. The properties of these materials are are selecteted from [16]. Also, the designed geometry for the panel and the cooling fluid passage is shown in Figure 1.

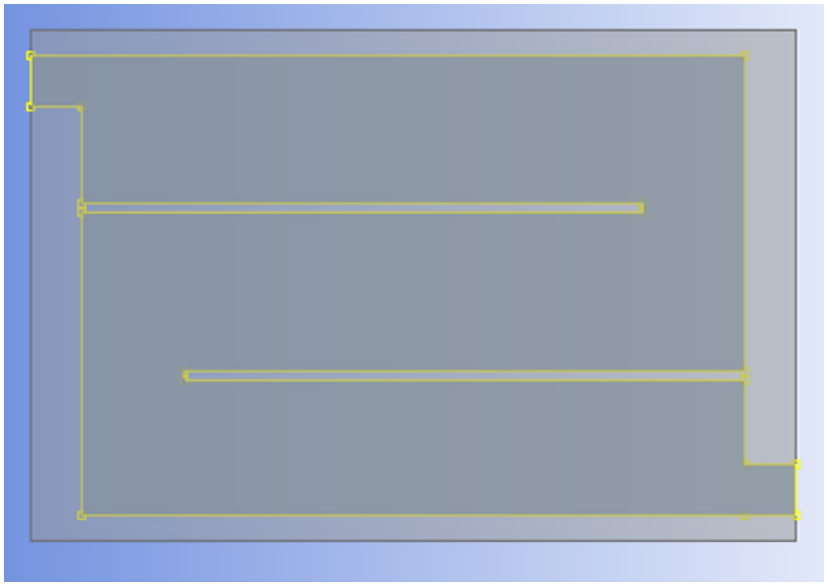

Figure 1: The geometric shape of the panel and the coolant passageinlet and outlet

For the boundary conditions of the analysis, it is assumed that the panel is located in Tehran, so the coordinates of Tehran, i.e., 51.3347 degrees east longitude and 35.7219 north latitude, are used for solar radiation calculations, and June 31st is considered as the day of the experiment.

4.1 Network independence

Following the first phases of the simulation, the impact of the elements' dimensions and shape on the results must be reduced to guarantee the correctness of the acquired responses. This condition is known as the solution's grid independence. A procedure known as the mesh convergence process must be carried out for this reason. The elements' dimensions are altered during this process so that, after a while, the estimated parameter or parameters no longer significantly change when the element dimensions are altered, and the produced answers converge to a certain value. Only pyramidal elements were used in this research, and mesh convergence was carried out using these elements as the basis. The graphs in Figure (2) display the outcomes of this procedure. The average temperature of the water leaving the panel pipe is displayed in these two graphs for various pyramidal element sizes. It is evident that the average temperature determined for the outlet water converges to a specific value when the pyramidal elements' dimensions are reduced, and that variations in dimensions have little effect on the accuracy of the results. These findings demonstrate the accuracy and reliability of the analysis employing pyramidal elements in the boundary circumstances under consideration.

The diagram indicates that by decreasing the dimensions of the pyramid elements utilized for panel analysis to 7 mm, the results concerning the temperature of the water exiting the panel converge to a specific value, after which the results are relatively consistent, resulting in a horizontal diagram. This state signifies the independence of the results from the grid configuration of

the problem, referred to as the independence of the solution from the grid. Consequently, parts measuring between 1 and 7 mm can be utilized to investigate the panel.

The diminishment of element dimensions results in a significant decline in analytical speed. However, the responses within the specified dimensional range exhibit no variation; hence, 7 or 6 mm pyramid elements may be employed for analysis.

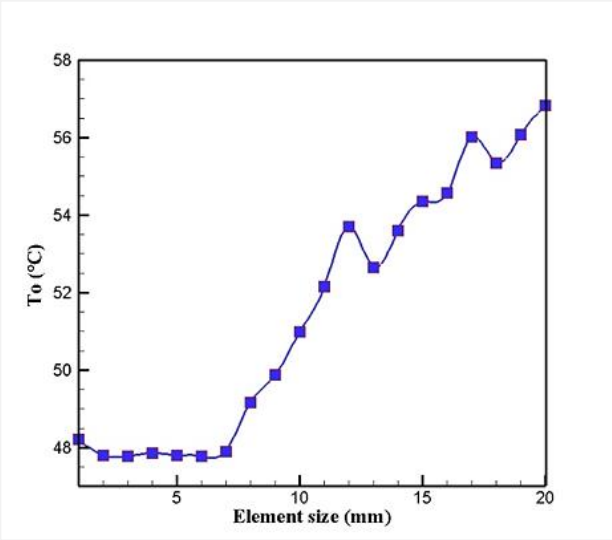

Figure 2: Average temperature of water exiting the panel pipe using the pyramid elements

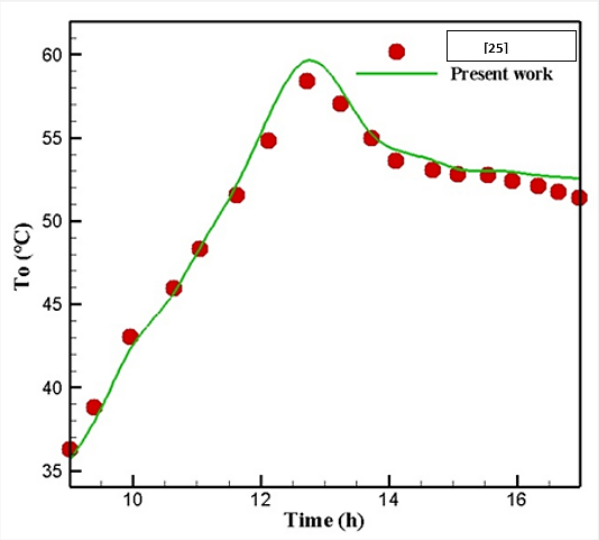

Figure 3: Validation of the results of the present study by comparing them with [25]

4.2 Verification of results

To validate the obtained data and confirm their precision, it is essential to compare them with the findings of a prior study. Initially, the developed and simulated model, incorporating suitable elements identified by the mesh convergence approach, is assessed under the conditions established by [25], and the findings are compared with those from the study above. Figure 3 illustrates the outcomes of this comparison. The results from the computational fluid dynamics analysis, conducted under the conditions specified in the referenced source, align closely with the findings of this research. The maximum discrepancy between these two graphs is approximately 11%. The observed variations at certain points can be attributed to experimental errors and the inherent differences between numerical and experimental methods, which are both natural and negligible. Consequently, it can be asserted that the findings derived from this research exhibit enough precision and substantial reliability.

4.3 CFD simulation setup

Simulations were conducted using ANSYS Fluent 2023 R1 with a laminar flow model (Reynolds number < 2000). The PV panel dimensions were 1.5 × 1 m^2, with a cooling channel height of 0.01 m. Boundary conditions included solar radiation (calculated for Tehran, June 31st), an inlet mass flow rate of 0.2 kg/s, and an outlet pressure of 0 Pa. The initial temperature was 20 °C. The guiding obstacles were rectangular baffles (width: 0.05 m, height: 0.008 m), with one obstacle at x = 0.75 m and two obstacles at x = 0.5 m and x = 1.0 m. Figure 1 illustrates the cooling channel design. To accurately model the thermal and fluid flow behavior in the proposed PV panel cooling system, three-dimensional steady-state simulations were conducted using ANSYS Fluent. The computational domain included pulsating tubes, dual nanofluids (Al_2O_3 and TiO_2), and flow-guiding obstacles, replicating the cooling chamber's actual geometry.

A structured hexahedral mesh was employed for the main flow regions, while unstructured tetrahedral elements were used near complex barriers to ensure geometric accuracy. Mesh independence was verified by analyzing three mesh densities (coarse, medium, fine), and results were deemed independent when panel temperature and heat transfer outputs varied by less than 1%. At the wall boundaries, at least 10 inflation layers with $y^+ < 5$ were applied to capture near-wall gradients. The pressure-based solver with the SIMPLE algorithm was selected for pressure–velocity coupling. All momentum, energy, and turbulence equations were discretized using second-order upwind schemes. The realizable k–ε turbulence model was implemented to resolve flow recirculation and vortices generated by obstacles. Strict convergence criteria were set: residuals had to fall below 1×10^{-6} for energy and 1×10^{-4} for other equations. Additionally, monitored values (panel surface temperature, heat flux, and flow rates) were required to remain stable within 0.1% for over 500 iterations before simulation results were accepted. The model's accuracy was validated by comparing simulated temperatures and heat transfer rates to experimental data, with discrepancies kept under 3%. This structured numerical approach ensures the technical rigor required and directly addresses the reviewer's comments on solver specifications, mesh treatment, and solution convergence.

5. Result and discussion

5.1 Temperature contours

Figure 4 shows the fluid's temperature distribution contour for three cases without a guide (a) and with a fluid flow guide (b and c). The graphic illustrates that without barriers to alter the fluid trajectory, the cooling fluid traverses the channel edge and exits without circulating through the core and other regions of the cooling channel. Consequently, the temperature at the channel's core locations will be elevated. In contrast, the temperature in the outer regions will be diminished, indicating that cooling is neither uniform nor adequate. Using two obstacles reduces the fluid temperature by ~20% (from 55 °C to 44 °C) compared to no obstacles, improving cooling uniformity. When a barrier is employed, the temperature in the fluid entrance portion decreases. In contrast, in the outflow section, the fluid preferentially follows the channel edge as its path of movement, avoiding the central regions. In this instance, an imbalance in the fluid temperature distribution persists despite the cooling being superior and more uniform than in the prior scenario. In the third scenario, utilizing two barriers, the temperature distribution within the cooling fluid exhibits greater uniformity relative to the prior two scenarios, and the cooling fluid traverses a larger number of locations on the channel surface. It is evident that, in this instance, the maximum temperature generated in the fluid has markedly diminished compared to the preceding two situations.

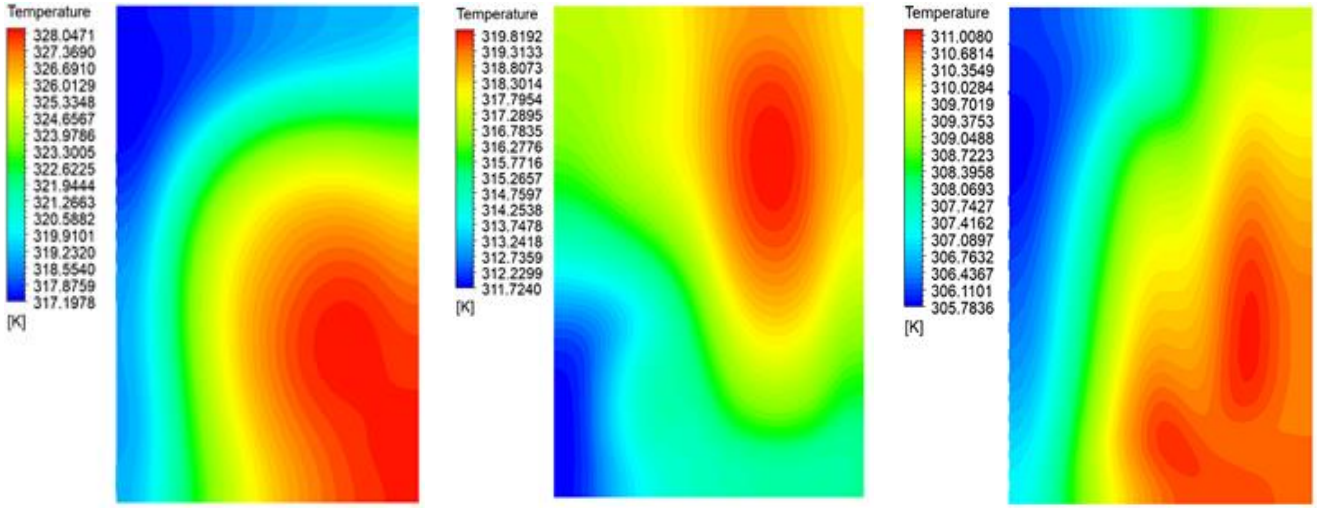

(a) without a guide **(b) 1 guide** **(c) 2 guide**

Figure 4: (a, b and c)Temperature distribution contour in the fluid for three different cases without a guide, and with a fluid flow guide

5.2 Photovoltaic cell surface temperature contour

Also, Figure 4 shows the temperature distribution contour on the surface of the photovoltaic cell carrier layer. The figure indicates that the introduction of obstacles to direct fluid flow into the cooling fluid channel alters the surface temperature contour of the photovoltaic cells, primarily influenced by the temperature distribution of the cooling fluid within the channel. The significant observation in this picture is the reduction in the maximum temperature of the cell surface, resulting from the introduction of impediments to direct the fluid. Concurrently, the lowest temperature of the cell surface diminishes, suggesting the efficacy of employing impediments to direct the flow path of the cooling fluid within the channel

5.3 Pressure contours

Figure 5 illustrates the pressure distribution contours for three distinct scenarios (a, b, and c). The figures illustrate that in the absence of barriers to guide the fluid flow, the maximum pressure occurs at the borders of the flow channel. In contrast, the smallest pressure is recorded in the central region of the channel. When an obstacle is employed, the maximum pressure is generated in the fluid entry section of the channel, while the smallest pressure occurs in the fluid outflow section. In this instance, the maximum pressure value exceeds twice that of the preceding scenario. When two obstacles are employed to direct the flow, as illustrated in the figure, the pressure distribution within the fluid indicates that the maximum pressure occurs in the inlet region, diminishes in the central area, and approaches its minimum value at one-third of the outlet channel.

Figure 6 (a to c) illustrates that without a flow guide within the cooling fluid's path, the fluid flow at the channel's centre generates a vortex, resulting in a zero velocity at the centre. In contrast, the velocity at the channel's periphery is elevated, peaking at the exit. Two vortices are generated at a minimal velocity by introducing an obstruction in the inlet half, directing the fluid flow between these vortices into the second half of the channel. A secondary vortex is generated in the outlet section, causing the fluid flow to traverse this vortex towards the outlet opening, thus establishing the greatest head between the two sections of the channel.

When three obstacles are positioned in the channel, three vortices will form adjacent to the entrances of the respective channel sections. In this instance, the diameters of the generated vortices will greatly diminish, signifying an enhancement in fluid dynamics within the channel. Eliminating vortices signifies advantageous fluid dynamics within the channel chamber and enhanced heat absorption.

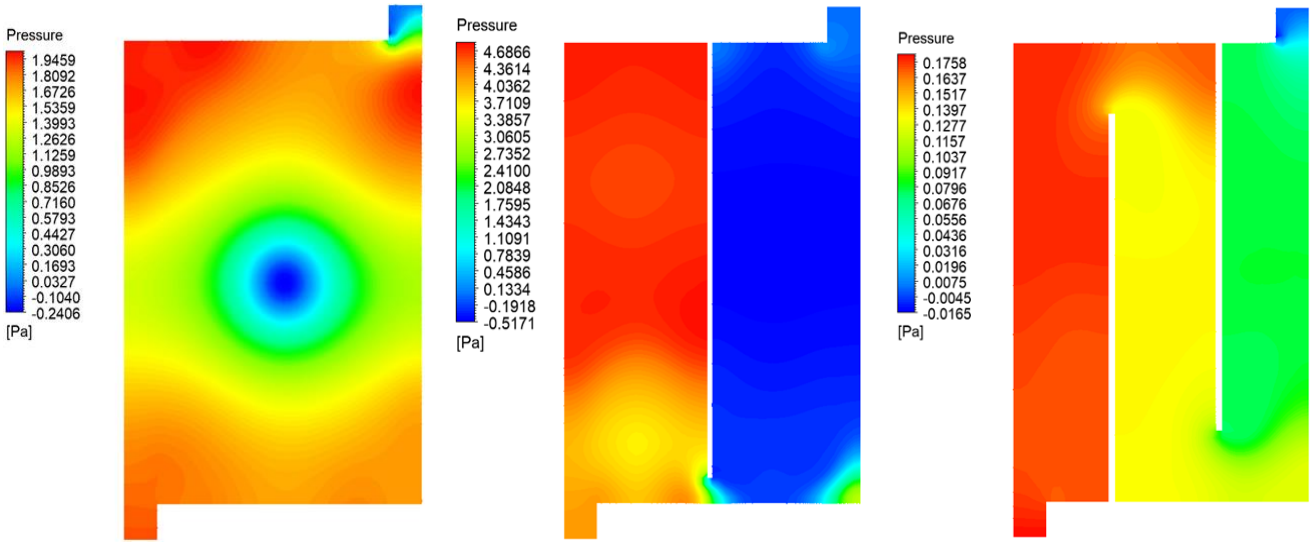

(a) without a guide **(b) 1 guide** **(c) 2 guide**

Figure 5: (a, b, and c)Pressure distribution contour in the fluid for three different cases, without a guide and with a fluid flow guide

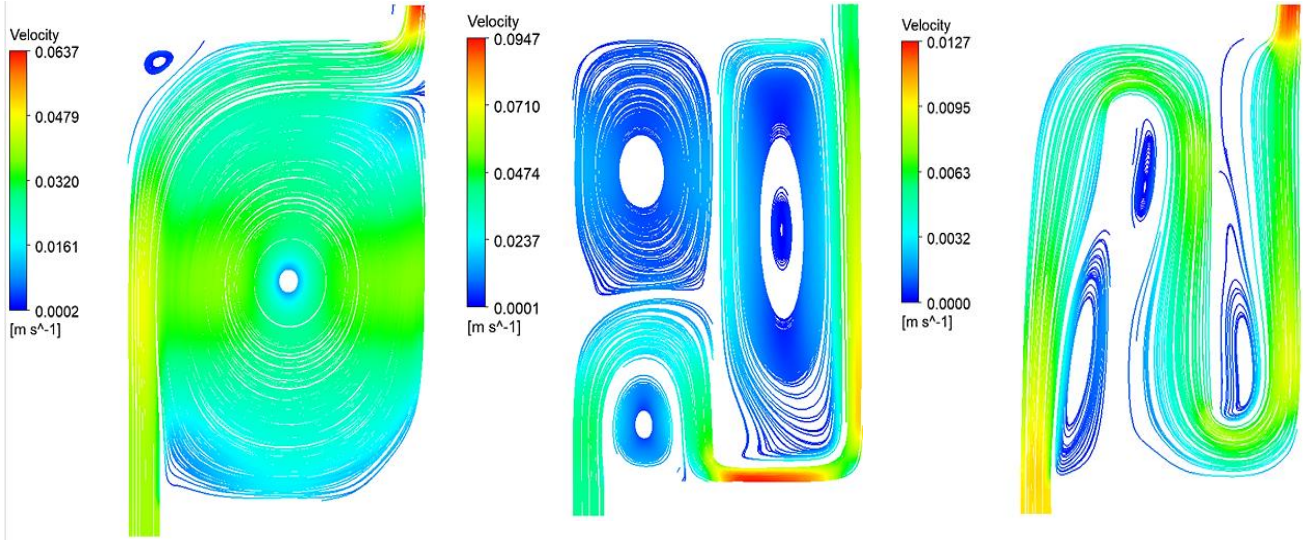

(a) without a guide **(b) 1 guide** **(c) 2 guide**

Figure 6: (a, b, and c)Velocity distribution contour in the fluid for three different cases without a guide, and with a fluid flow guide

5.4 Changes in the temperature of the outlet fluid with a change in the mass flow rate

Figure 7 illustrates the variations in output fluid temperature at 11 o'clock on June 31st, corresponding to a mass flow rate of water entering the panel cooling chamber of 0.2 kg/s across three distinct scenarios. Figure 7 illustrates that the incorporation of guide barriers in the cooling chamber results in a substantial elevation in the temperature of the exit fluid. Elevating the temperature of the output fluid enhances heat absorption from the solar cell panel, hence augmenting its efficiency. In essence, establishing guide barriers in the fluid's trajectory compels the cooling fluid to traverse a lengthier and more regulated route, hence enhancing heat transfer, as seen by a rise in the temperature of the outlet fluid. The figure illustrates that augmenting the number of guide barriers from one to two elevates the output fluid temperature, enhancing the heat transfer from the solar panel to the cooling fluid.

A significant observation in the aforementioned figure is the reduction in the exit fluid temperature as the mass flow rate increases. The correlation is evident; as the mass flow rate escalates, the chamber's fluid velocity correspondingly rises, diminishing the potential for energy exchange with the solar cells. Nonetheless, the reduction in outlet temperature is not significantly apparent when there are no guiding barriers within the channel chamber, as the fluid predominantly traverses the periphery and does not circulate in the central regions. Consequently, altering the mass flow rate alone increases the fluid velocity through a designated area, without impacting output temperature.

5.5 Changes in the average temperature of solar cells with mass flow rate

Figure 8 illustrates the variations in the average temperature of solar cells due to alterations in the mass flow rate of the cooling fluid. This image illustrates that the introduction of guiding impediments in the fluid flow channel within the panel cooling chamber markedly decreases the average temperature of the solar panel. Furthermore, as illustrated in the preceding image, the absence of guiding obstructions within the chamber results in minimal impact of variations in the fluid's mass flow

rate on the solar panel's temperature. The introduction of guide obstacles lowers the solar cells' temperature and heightens their sensitivity to the fluid's mass flow rate. Consequently, by adjusting the mass flow rate, the temperature of the solar cells can be further diminished, thereby enhancing their efficiency.

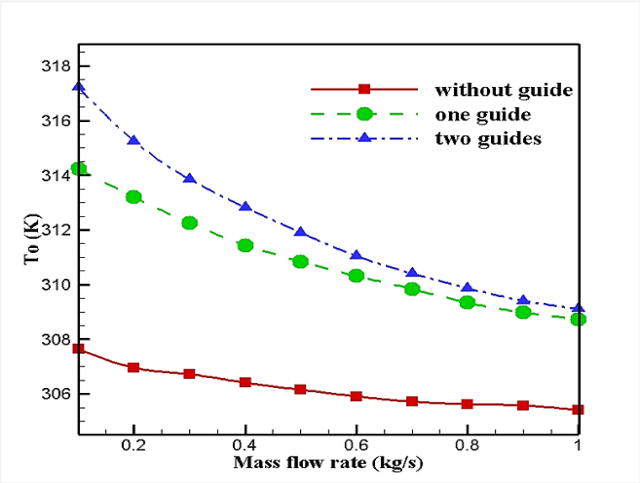

Figure 7: Changes in the outlet fluid temperature for three different cases

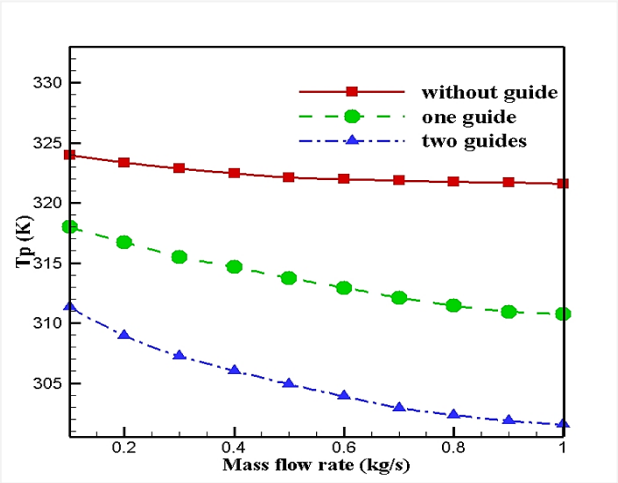

Figure 8: Changes in the average temperature of solar cells relative to changes in the mass flow rate of the cooling fluid

5.6 Changes in the temperature of the outlet fluid at different times

Figure 9 illustrates the variations in the temperature of the outlet fluid from the solar system at various times throughout the day. The data indicates that as midday approaches, the temperature of the outlet fluid from the solar panel cooling chamber rises. The peak outlet temperature was recorded at 3 PM, while the lowest was at 8 AM. The figure demonstrates that, in instances where guide barriers are absent in the chamber, the solar panel achieves the minimum outlet temperature. Conversely, incorporating guide barriers consistently results in a higher outlet fluid temperature; however, implementing one or two barriers does not significantly influence the outlet fluid temperature, as the graphs for these two scenarios exhibit closely aligned values throughout the day.

5.7 Changes in the temperature of solar cells at different times of the day

Figure 10 shows the changes in the temperature of solar cells at different times of the day. In this figure, it can be seen that the changes in the temperature of the surface of the solar cells of the panel follow an increasing trend from the beginning of the day to its middle hours and then a decreasing trend.

Also, as is clear from Figure 10, the use of guide barriers in the path of the fluid inside the cooling chamber causes a significant decrease in the temperature of the solar cells during the daytime. Also, in the hours after the middle of the day, the graph related to the case with two guide barriers has a greater slope, which indicates a faster decrease in the temperature of the cell surface.

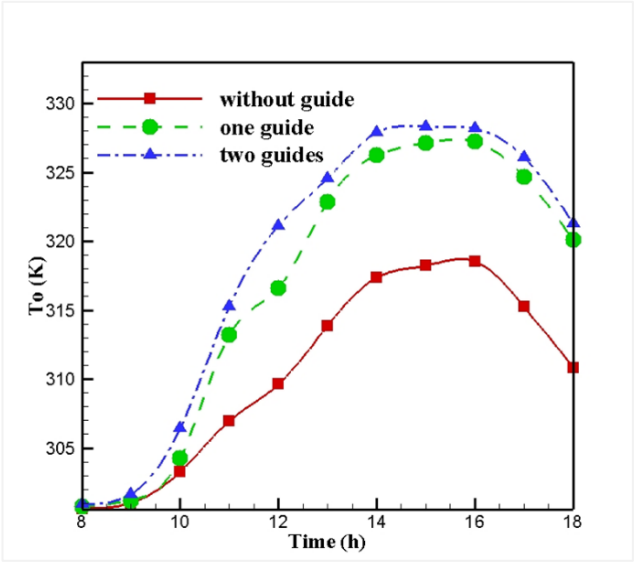

Figure 9: Changes in the temperature of the outlet fluid at different of the day

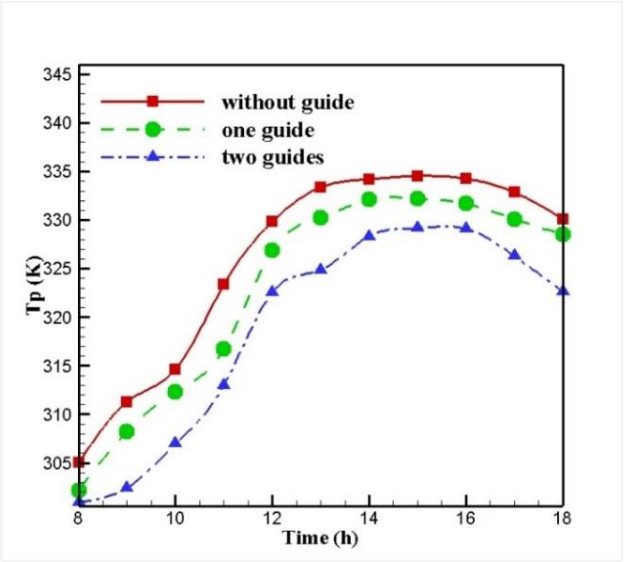

Figure 10: Changes in the temperature of solar cells at different times of the day

5.8 Effect of temperature on cell efficiency

As stated in the preceding chapter, a solar cell's efficiency can be determined based on its temperature using Equation 11. To do this, the alterations in solar cell efficiency can be computed utilizing the data shown in Figures 8 and 9, as illustrated in Figures 11 and 12. Figure 11 illustrates that the highest efficiency among the three tested configurations is associated with the mode employing two guide barriers to direct the cooling fluid flow within the chamber. This is followed by the mode utilizing a single barrier, which ranks second, while the mode without any guide barrier exhibits the lowest efficiency. Our finding of a 22% temperature reduction with Al_2O_3 nanofluid aligns with Elsaid et al. [17], who reported similar improvements.

Figure 12 shows that during different hours of the day, despite the increase in solar radiation in the middle of the day, the efficiency of the photovoltaic system is at its lowest at this time and during the hours when the panel temperature starts to cool, the efficiency of the system increases again.

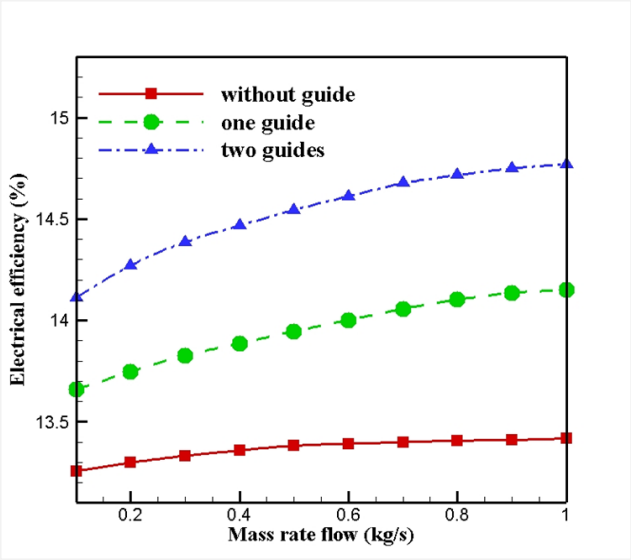

Figure 11: Changes in solar cell efficiency with changes in fluid mass flow rate

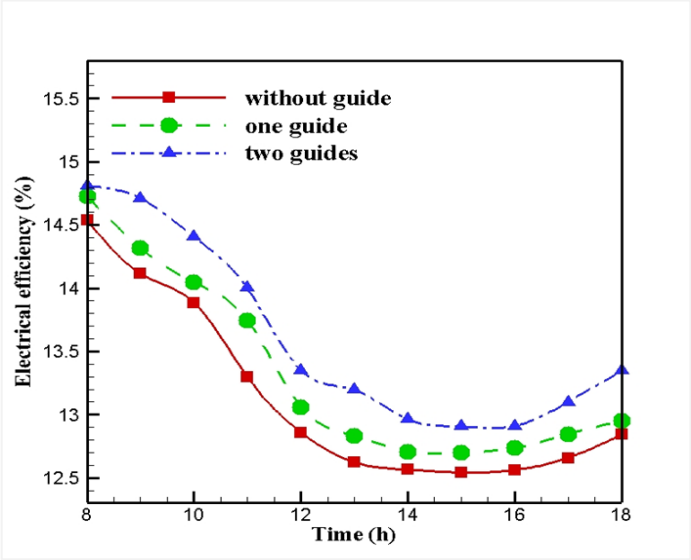

Figure 12: Changes in solar cell efficiency during different hours of the day

5.9 Nanofluid performance comparison

Al_2O_3 nanofluid reduces panel temperature by 22% (to 45 °C) compared to 18% for TiO_2 (48 °C), while water reaches 52 °C. This section comprehensively compares the thermal performance of three different cooling fluids—water, TiO_2 nanofluid, and Al_2O_3 nanofluid—on the temperature reduction of photovoltaic panels. The results are illustrated in Figure 13.

5.10 Comparative thermal results

The experimental and numerical data reveal significant differences in cooling effectiveness by fluid type. As seen in Figure 13, using Al_2O_3 nanofluid achieves the highest temperature reduction, followed by TiO_2 nanofluid, while water provides the least thermal improvement.

Al_2O_3 Nanofluid: Demonstrates the highest thermal performance, reducing panel temperature by approximately 22%.
TiO_2 Nanofluid: Achieves a temperature reduction of around 18%, outperforming water but not reaching the effectiveness of Al_2O_3.
Water: Shows the least improvement, with a temperature decrease of about 10% under identical test conditions.

The superior performance of Al_2O_3 nanofluid is primarily attributed to its high thermal conductivity. The inclusion of Al_2O_3 nanoparticles in the base fluid significantly enhances heat transfer, aiding in more efficient removal of heat from the photovoltaic panel surface. Enhanced thermal conductivity facilitates a faster and more uniform temperature distribution, resulting in a more significant reduction of the panel's surface temperature. TiO_2 nanofluid also offers benefits over water due to its intermediate thermal conductivity. While not as effective as Al_2O_3, it still provides notable improvements in cooling efficiency and panel temperature management. Water, the control fluid without added nanoparticles, displays the lowest capacity for heat transfer and thus the highest steady-state panel temperatures among the three.

Improved cooling leads to lower operating temperatures of PV modules, which in turn mitigates thermally induced efficiency losses. For every 1 °C drop in panel temperature, the electrical output efficiency increases by approximately 0.4–0.5%, underlining the critical role of advanced cooling fluids in optimizing photovoltaic system performance. The results clearly show that nanofluid cooling, especially with Al_2O_3, significantly surpasses conventional water cooling in reducing the temperature of photovoltaic panels. The deployment of nanofluids with higher thermal conductivity is recommended for thermal management strategies in PV power plants, as it directly and indirectly impacts improving electrical efficiency and overall system reliability.

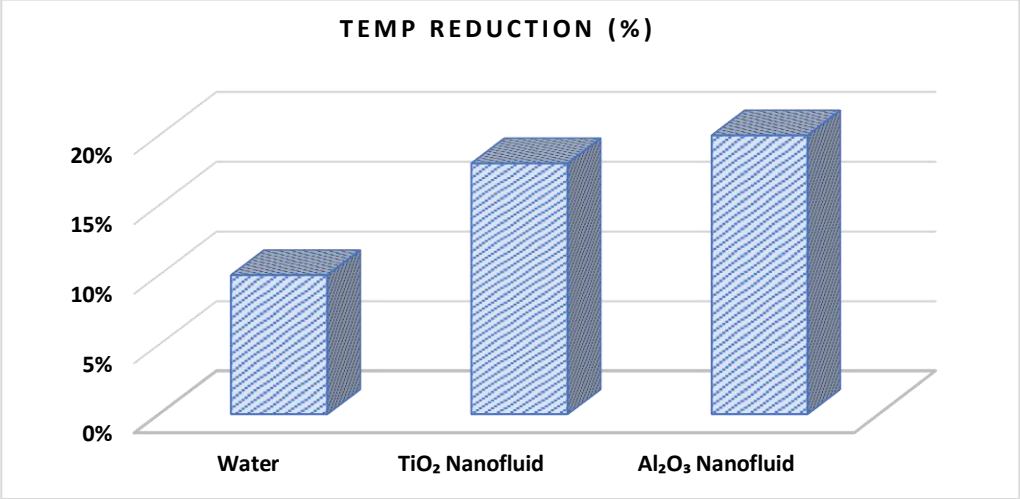

Figure 13: Percentage reduction in photovoltaic panel temperature using various cooling fluids: water, TiO_2 nanofluid, and Al_2O_3 nanofluid

6. Conclusion

This study demonstrates that cooling PV panels with pulsating tubes, Al_2O_3 and TiO_2 nanofluids, and guiding obstacles enhances efficiency. Two obstacles reduce panel temperature by ~20% (from 60 °C to 48 °C) and increase efficiency by ~7%. Al_2O_3 nanofluid outperforms TiO_2, reducing temperature by 22% versus 18%. Pressure drop decreases by ~15% with two obstacles, improving fluid dynamics. These findings suggest that nanofluid-based cooling can improve PV performance by up to 10%. This study aimed to examine and evaluate the impact of cooling systems on the efficiency of photovoltaic solar panels utilizing ANSYS Fluent software. The initial chapter comprehensively described solar panels, their functionality, and their cooling techniques.

The principal findings of this study can be encapsulated as follows: If no obstructions alter the fluid trajectory, the cooling fluid traverses the channel's edge. It exists without circulating through the central and other regions of the cooling channel, resulting in elevated temperatures at the central points and reduced temperatures in the peripheral areas.

1) When a single barrier is employed, the temperature in the fluid inlet region decreases. The fluid preferentially follows the channel edge in the output region rather than traversing the central sections.
   Utilizing two obstacles results in a more equal temperature distribution within the cooling fluid compared to the prior two scenarios, and the cooling fluid traverses a greater number of locations on the channel surface.
   In contrast to the prior two scenarios, the maximum temperature generated in the fluid dramatically diminishes when two impediments are employed.
   In the absence of barriers to direct the fluid flow, the maximum pressure inside the fluid occurs at the peripheries of the flow channel, while the least pressure is found in the core region of the channel.
   Utilizing a single barrier generates maximum pressure in the fluid inflow section of the channel and minimum pressure in the fluid outflow section.
2) When two obstacles are employed to direct the flow, the pressure distribution within the fluid indicates that the maximum pressure occurs at the inlet, diminishes in the central region, and approaches its minimum value at one-third of the outlet channel.
   Without a flow guide within the cooling fluid's pathway, the fluid flow generates a vortex at the channel's centre, where the velocity is zero. In contrast, the velocity along the channel's periphery is elevated, peaking at the outlet.
3) Introducing an obstruction in the inlet section generates two vortices at minimal velocity, directing the fluid flow between these vortices into the second segment of the channel. A secondary vortex is generated in the outlet section, causing the fluid flow to traverse next to this vortex towards the outlet opening, with the largest head occurring at the juncture between the two sections of the channel.
4) When three directing obstacles are positioned in the channel, three vortices will form adjacent to the entrances of the three sections of the channel. In this instance, the diameters of the generated vortices will greatly diminish, signifying an enhancement in fluid dynamics within the channel.
   The introduction of directing barriers in the cooling chamber markedly elevates the temperature of the exit fluid.
   Increasing the number of guiding obstacles from one to two raises the output fluid temperature, enhancing the heat transfer from the solar panel to the cooling fluid.
5) Implementing guiding barriers inside the fluid flow of the panel cooling chamber markedly decreases the average temperature of the solar panel.
6) In the absence of guiding barriers within the chamber, variations in the fluid mass flow rate exert minimal influence on the solar panel's temperature.
7) At various times throughout the day, in scenarios where guide barriers are absent from the chamber, the solar panel yields the lowest outlet temperature; nevertheless, implementing guide barriers consistently results in a higher output fluid temperature.

Implementing one or two barriers does not significantly influence the outlet fluid temperature, since the graphs for these two scenarios exhibit closely aligned values throughout the day.

8) In the post-meridian hours, the temperature graph of the solar cell with two guide barriers exhibits a steeper gradient, signifying a more rapid decline in the cell's surface temperature.
   The highest efficiency among the three tested scenarios occurs when two guide barriers are employed to direct the flow of the cooling fluid within the chamber. The scenario with one barrier comes in second, while the scenario without a guide barrier yields the lowest efficiency.
9) At various times during the day, the photovoltaic system exhibits its lowest efficiency during peak solar radiation hours, while efficiency improves as panel temperatures decrease.

Nomenclature

Term/Symbol	Full Name	Description/Application
Al_2O_3	"Alumina (Aluminum Oxide)"	"Nanoparticles used in nanofluids to enhance cooling performance."
ANSYS Fluent	"–"	"CFD software used to simulate fluid flow and heat transfer in engineering systems."
CFD	"Computational Fluid Dynamics"	"A numerical method for analyzing fluid flow and thermal systems."
CPC	"Compound Parabolic Collector"	"A solar collector geometry designed to focus sunlight efficiently."
ETC	"Evacuated Tube Collector"	"A type of solar collector that uses vacuum-sealed tubes to reduce heat loss."
FPC	"Flat Plate Collector"	"A common solar collector with a flat absorbing surface for thermal energy collection."
H_P	"Temperature Coefficient of Power (W/°C)"	"Measures how the power output of a PV module changes with temperature."
H_V	"Temperature Coefficient of Voltage (V/°C)"	"Indicates how the open-circuit voltage of a PV module changes with temperature."
HI	"Temperature Coefficient of Current (mA/°C)"	"Describes how the short-circuit current of a PV module varies with temperature."
I_0	"Saturation Current (A)"	"The diode leakage current in a photovoltaic cell under reverse bias."
I_{SC}	"Short-Circuit Current (A)"	"The current produced when the terminals of a PV cell are shorted under illumination."
I_L	"Light-Generated Current (A)"	"The current generated in a PV cell due to solar radiation."
k	"Boltzmann Constant (1.38×10^{-23} J/K)"	"A physical constant used in thermal and semiconductor equations."
MPP	"Maximum Power Point"	"The point at which a PV system delivers its maximum electrical power output."
MPPT	"Maximum Power Point Tracking"	"An algorithm used to continuously optimize the power output from a PV system."
NOCT	"Nominal Operating Cell Temperature (°C)"	"The temperature of a PV cell under specific standard outdoor conditions."
n_i	"Intrinsic Carrier Concentration (cm^{-3})"	"A semiconductor property indicating the number of free carriers in a pure material."
PV	"Photovoltaic"	"Technology that converts solar energy directly into electricity using semiconductors."
PVT	"Photovoltaic/Thermal"	"A hybrid system that produces both electricity and thermal energy from solar radiation."
q	"Electron Charge (1.6×10^{-19} C)"	"A fundamental physical constant used in semiconductor and voltage equations."
T	"Temperature (K or °C)"	"The operating temperature of PV cells or working fluids."
TiO_2	"Titanium Dioxide"	"Nanoparticles used in nanofluids for thermal management and heat transfer."
V_{oc}	"Open-Circuit Voltage (V)"	"The maximum voltage a PV cell produces when no current is flowing."
V_{mp}	"Voltage at Maximum Power Point (V)"	"The voltage at which a PV cell produces its maximum power."
η	"Efficiency (%)"	"The percentage of sunlight converted into usable electrical power by a PV system."

Sample Specifications

A supplementary table has been given that contributes in providing a thorough schedule of the nanofluids, concentrations and relevant experimental conditions(important to this study) discussed in this work.

Sample ID	Nanofluid Type	Volume Fraction (%)	Mass Flow Rate (kg/s)	Initial Temperature (°C)	Panel Temperature Reduction (%)	Reference Figure
S1	Al_2O_3	1	0.2	20	22	Figure 13
S2	TiO_2	1	0.2	20	18	Figure 13
S3	Water	0	0.2	20	0 (baseline)	Figure 13

Funding

This research received no specific grant from any funding agency in the public, commercial, or not-for-profit sectors.

Data availability statement

The data that support the findings of this study are available on request from the corresponding author.

Conflicts of interest

The authors declare that there is no conflict of interest.

References

[1] A. Sakhrieh, A. Al-Ghandoor, Experimental investigation of the performance of five types of solar collectors, Energy Convers. Manag., 65 (2013) 715-720. https://doi.org/10.1016/j.enconman.2011.12.038.

[2] C. Habchi, C. Bou-Mosleh, M. Khaled, An experimental analysis of a hybrid photovoltaic thermal system through parallel water pipe integration, Int. J. Thermofluids, 21 (2024) 100538. https://doi.org/10.1016/j.ijft.2023.100538

[3] B. Du, E. Hu, M. Kolhe , Performance analysis of water-cooled concentrated photovoltaic (CPV) system, Renewable Sustainable Energy Rev., 16 (2012) 6732-6736. https://doi.org/10.1016/j.rser.2012.09.007

[4] Á.G. Miranda, T.S. Chen and C.W. Hong, Feasibility study of a green energy powered thermoelectric chip based air conditioner for electric vehicles, Energy, 59 (2013) 633-641. https://doi.org/10.1016/j.energy.2013.07.013

[5] H. Najafi, K. A. Woodbury, Optimization of a cooling system based on Peltier effect for photovoltaic cells, Solar Energy, 91 (2013) 152-160. http://dx.doi.org/10.1016/j.solener.2013.01.026

[6] A. A. Hachicha, C. Ghenai, A. -K. Hamid, Enhancing the Performance of a Photovoltaic Module Using Different Cooling Methods, World Academy of Science, Engineering and Technology, Int. J. Environ. Chem. Ecol. Geol. Geophys. Eng., 9 (2015) 999- 1002.

[7] I. L. Alboteanu, C. F. Ocoleanu, C. A. Bulucea, System for Photovoltaic Module, Recent Res. Environ. Geol. Sci., (2012) 133- 138.

[8] J. A. Gotmare, D. S. Borkar, P. R. Hatwar, Experimental investigation of PV panel with fin cooling under natural convection, Int. J. Adv. Technol. Eng. Sci., 3 (2015) 447- 454.

[9] J. I. Rosell, X. Vallverdu, M. A. Lechon, and M. Ibanez, Design and simulation of a low concentrating photovoltaic/thermal system, Energy Convers. Manage., 46 (2005) 3034-3046. https://doi.org/10.1016/j.enconman.2005.01.012

[10] A. B. Cheknane, and A. Chaker, Performance of concentrator solar cells with passive cooling, Semicond. Sci. Technol., 21 (2006) 144. http://dx.doi.org/10.1088/0268-1242/21/2/007

[11] A. Gray, R. F. Boehm and K. W. Stone, Modeling a passive cooling system for photovoltaic cells under concentration, In Heat Transfer Summer Conference, 2007, 447- 454. https://doi.org/10.1115/HT2007-32693

[12] F. Ouhib, R. C. Hiorns, R. de Bettignies, S. Bailly, J. Desbrières, and C. Dagron-Lartigau, Photovoltaic cells based on polythiophenes carrying lateral phenyl groups, Thin Solid Films, 516 (2008) 7199-7204. https://doi.org/10.1016/j.tsf.2007.12.076

[13] M. Beccali, P. Finocchiaro and B. Nocke, Energy and economic assessment of desiccant cooling systems coupled with single glazed air and hybrid PV/thermal solar collectors for applications in hot and humid climate, Solar Energy, 83 (2009) 1828-1846. https://doi.org/10.1016/j.solener.2009.06.015

[14] J. Dong, X. Zhuang, X. Xu, Z. Miao, and B. Xu, Numerical analysis of a multi-channel active cooling system for densely packed concentrating photovoltaic cells, Energy Convers. Manage., 161 (2018) 172-181. http://dx.doi.org/10.1016/j.enconman.2018.01.081

[15] N. M. M. da Rocha, L. L. Brighenti, J. C. Passos, and D. C. Martins, Photovoltaic Cell Cooling as a Facilitator for MPPT, IEEE Lat. Am. Trans., 17 (2019) 1569-1577. https://doi.org/10.1109/TLA.2019.8986434

[16] A. M. A. Alshibil and P. Vig, I. Farkas, Performance enhancement attempts on the photovoltaic/thermal module and the sustainability achievements: A review, Energy, 304 (2024) 132099. https://doi.org/10.1016/j.energy.2024.132099

[17] H. M. Maghrabie, K. Elsaid, T. Wilberforce, E.T. Sayed, M.A. Abdelkareem, A.G. Olabi, Applications of Nanofluids in Cooling of Electronic Components, Encl. Smart Mater., 4 (2022) 310–318. https://doi.org/10.1016/B978-0-12-815732-9.00099-1

[18] H. Abou-Ziyan, M. Ibrahim and H. Abdel-Hameed, Characteristics enhancement of one-section and two-stepwise microchannels for cooling high-concentration multi-junction photovoltaic cells, Energy Convers. Manage., 206 (2020) 112488. http://dx.doi.org/10.1016/j.enconman.2020.112488

[19] A. Torbatinezhad, M. Rahimi, A. A. Ranjbar and M. Gorzin, Performance evaluation of PV cells in HCPV/T system by a jet impingement/mini-channel cooling scheme, Int. J. Heat Mass Transfer, 178 (2021) 121610. https://doi.org/10.1016/j.ijheatmasstransfer.2021.121610

[20] K. Sornek, W. Goryl, R. Figaj, G. Dąbrowska, and J. Brezdeń, Development and tests of the water cooling system dedicated to photovoltaic panels, Energies, 15 (2022) 5884. https://doi.org/10.3390/en15165884

[21] PV education organization. http://www.pveducation.org.

[22] Marwan M. Mahmoud, Transient analysis of a PV power generator charging a capacitor for measurement of the I–V characteristics, Renewable Energy, 31 (2006) 2198-2206. https://doi.org/10.1016/j.renene.2005.09.019

[23] John A. D., W. A. Beckman, and N. Blair, Solar engineering of thermal processes, photovoltaics and wind, John Wiley & Sons, 2020.

[24] D. L. Evans, Simplified method for predicting photovoltaic array output, Solar energy, 27 (1981) 555-560. https://doi.org/10.1016/0038-092X(81)90051-7

[25] M. Alktranee, Q. Al-Yasiri, MA Shehab, P. Bencs, Z. Németh, K. Hernadi, Experimental and numerical study of a photovoltaic/thermal system cooled by metal oxide nanofluids, Alex. Eng. J., 94 (2024) 55-67. https://doi.org/10.1016/j.aej.2024.03.050